Pumped thermal grid storage with heat exchange

Robert B. Laughlin

Citation: Journal of Renewable and Sustainable Energy **9**, 044103 (2017);
View online: https://doi.org/10.1063/1.4994054
View Table of Contents: http://aip.scitation.org/toc/rse/9/4
Published by the American Institute of Physics

Pumped thermal grid storage with heat exchange

Robert B. Laughlin[a)]
Department of Physics, Stanford University, Stanford, California 94305, USA

(Received 3 July 2017; accepted 5 July 2017; published online 2 August 2017)

A thermal heat-pump grid storage technology is described based on closed-cycle Brayton engine transfers of heat from a cryogenic storage fluid to molten solar salt. Round-trip efficiency, computed as a function of turbomachinery polytropic efficiency and total heat exchanger steel mass, is found to be competitive with that of pumped hydroelectric storage. The cost per engine watt and cost per stored joule based are estimated based on the present-day prices of power gas turbines and market prices of steel and nitrate salt. Comparison is made with electrochemical and mechanical grid storage technologies. [http://dx.doi.org/10.1063/1.4994054]

I. INTRODUCTION

It is widely understood that facilities for storing very large amounts of electric energy are key to any long-term plan to supplant fossil fuel with renewable energy.[1–3] The desirability of switching to renewable sources is, of course, controversial, and it is not clear that eliminating fossil fuel is economically feasible at this time.[4–7] But without storage, it is also impossible.[8] The intermittencies of energy sources like wind and sun are fundamentally incompatible with the electricity industry's need to supply power to customers—the instant demands by customers. The overriding importance of timing is demonstrated by the frequent development of negative spot prices for electric energy in markets with large wind deployments.[9–12]

The purpose of this paper is to discuss a specific storage technology and make the case that it has the right engineering compromises to prevail when the need for storage eventually becomes acute. It is an implementation of pumped thermal storage, an idea already in the literature and under development in industry, and differs from others chiefly in the substitution of heat exchangers for thermoclines[13–17] (Fig. 1). Instead of pumping water uphill from a low reservoir to a higher one to store energy, as occurs in pumped hydroelectricity, one pumps heat from a cold body to a hot one by means of a heat engine. In either case, the process is reversible so that energy banked can be withdrawn later to satisfy demand.

The reasoning leading to the "Brayton Battery," as it might be called, applies the metrics of safety, low cost, and high efficiency, *in this order*. The average power delivered to a large metropolitan area such as Los Angeles or New York is about 1.4×10^{10} W.[18] Storing this power for only one hour gives 5.04×10^{13} J or one Hiroshima-sized atomic bomb.[19] It is absolutely essential that explosive release of this stored energy be physically impossible. Once this safety criterion is met, capital and maintenance costs must be brutally minimized, even at the price of a small hit in round-trip efficiency, because storage of electricity is fundamentally about value, not about conserving energy.

The round-trip storage efficiency η_{store} of the configuration in Fig. 1 satisfies

$$\eta_{store} < 1 - \frac{2T_{dump}}{T_1 - T_0}\left(\frac{1}{\eta_c} - \eta_t\right)\frac{\ln(\xi)}{\xi - 1}, \tag{1}$$

[a)]URL: http://large.stanford.edu

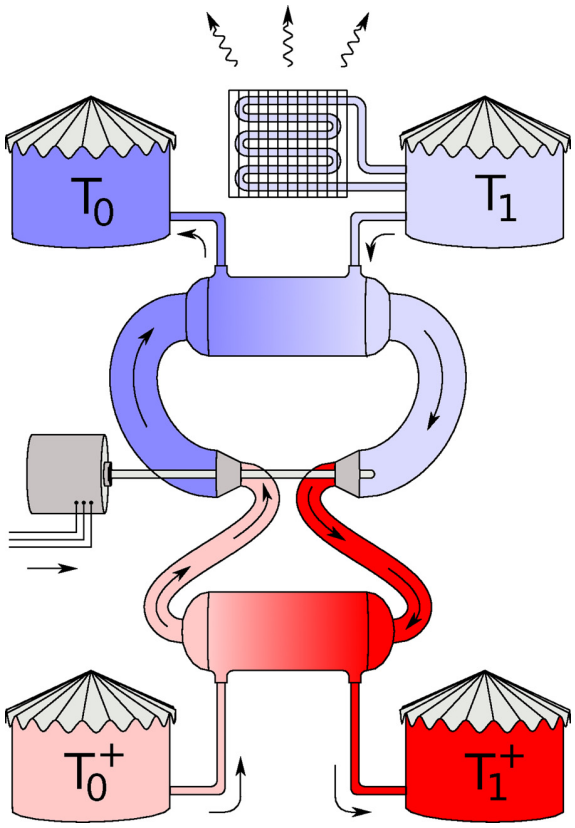

FIG. 1. Conceptual diagram of pumped thermal storage with heat exchange. Heat is added to/removed from the working fluid of a closed-cycle Brayton engine by means of heat exchangers with counterflowing storage fluids. In the base case, the working fluid is Ar gas, and the heat storage media are molten salt (high pressure side) and a hydrocarbon liquid (low pressure side). The media are stored in four tanks at different temperatures constrained by the condition $T_0^+/T_0 = T_1^+/T = \xi$. In the limit that the turbine-compressor pair is perfectly adiabatic and the heat exchangers are very large, the engine is fully reversible. Nonideality in both the turbomachinery and the heat exchangers generates entropy that must be sloughed into the environment as waste heat. This loss leads to the round-trip efficiency bound given in Eq. (1).

where η_c and η_t are the polytropic efficiencies of the compressor and turbine, respectively, and T_{dump} is the (Kelvin) temperature at which waste heat is sloughed. For the prototype parameters in Table I, this limit is 0.75. The factor of 2 in Eq. (1), which comes from the need to pass the working fluid through the turbomachinery twice in each storage cycle, is the efficiency disadvantage vis-à-vis pumped hydroelectricity or thermoclines.

The structure of this paper is as follows. Section II discusses materials, with emphasis on the properties of steels and storage fluids and the constraints these impose on operating temperatures. Section III deals with regeneration, the need for which follows from the material constraints. Section IV presents a detailed round-trip efficiency computation. Section V discusses costs. Section VI gives the summary.

II. MATERIALS

A. Steel limitations

Closing the Brayton cycle as shown in Fig. 1 enables the background working fluid pressure to be raised, thus greatly reducing the cost per engine watt. The turbine rotation speed and blade angles fix the working fluid velocity to first approximation, and thus, increasing the pressure simply increases the number of moles of working fluid passing a given point per second and thus the total power. Background pressures as high as 7.7×10^6 Pa (77 atmospheres) compressed to 1.38×10^7 Pa have been experimentally benchmarked in closed-cycle Brayton

TABLE I. Prototype design parameters assumed throughout this paper. The differences between charge and discharge are ignored for clarity, as is the need to make T_{dump} higher than ambient to slough heat effectively. The compressor polytropic efficiency η_c is the ratio of ideal compressive work to actual work in the limit of small compression (i.e., for a single stage). The turbine polytropic efficiency η_t is the inverse of this ratio in the limit of small expansion. These particular values η_c and η_t are industry standards discussed further in Sec. IV B.[59–63]

	Ar	N_2
T_0	180 K	180 K
T_0^+	300 K	300 K
T_1	495 K	495 K
T_1^+	823 K	823 K
$T_{\rm dump}$	300 K	300 K
ξ	1.66	1.66
$\eta_{\rm c}$	0.91	0.91
$\eta_{\rm t}$	0.93	0.93
p_0	1.00×10^5 Pa	1.00×10^5 Pa
$p_{\rm l}$	1.00×10^6 Pa	1.00×10^6 Pa
$p_{\rm h}$	3.55×10^6 Pa	6.52×10^5 Pa

engines using supercritical CO_2.[20] Pressures approaching 3.0×10^7 Pa (300 atm) are routine in modern supercritical steam power plants.[21]

However, the use of high pressure severely limits the temperatures that one can employ. As shown in Fig. 2, raising the temperature of a steel eventually causes it to exhibit creep, a slow plastic deformation that presages full mechanical failure at higher temperatures. This effect is irrelevant on short time scales but is a major design constraint on the scale of 40 years.[22] Creep is what prevents conventional carbon steels from being used in high-pressure thermal applications at temperatures above about 700 K (427 °C). This limit can be raised to about 800 K (527 °C) by adding impurities in percent amounts that block grain boundary motion, but maximum resistance to creep requires full alloying with Cr and Ni to make stainless steels.[22] The creep limitations of alloy steels may be seen from Fig. 2 to apply universally, including to Inconels. Thus, pressure vessels constructed from steel become problematic for

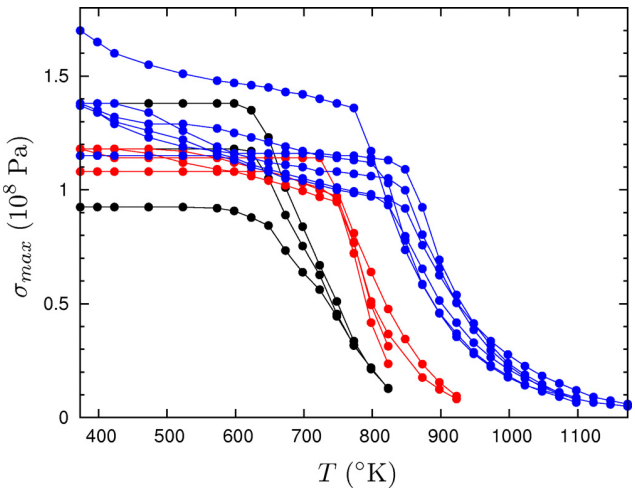

FIG. 2. Maximum steel stress allowed by the 2007 ASME Boiler and Pressure Vessel Code, Part II, Section D, Tables 1A and 1B for a representative selection of steels (seamless tubing).[22] The "creep cliff" at $T = 873$ K (600 °C) is clearly visible. Black: Carbon steels, UNS Nos. K01201, K02707, and K03501. Red: Low-alloy steels, UNS Nos. K11522, K11547, K11597, and K21590. Blue: Stainless steels, UNS Nos. S30409, S30815, S31609, S32109, S34709, and N08810 (Incalloy 800H).

temperatures much above 873 K (600 °C). This is a major consideration in present-day supercritical steam plants.[21]

B. Solar salt

The temperature limitations of steels make solar salt, the elementary $NaNO_3/KNO_3$ eutectic storage medium of the concentrating solar industry, to be a particularly good choice for the high-temperature storage medium.[23–25] All solid and liquid substances have heat capacities of approximately $3R$ per mole of atoms, where R is the ideal gas constant, in the temperature range of interest, so virtually, anything will act as a thermal storage medium, including rocks. However, the cost of either gravel or salt is much less than the cost of the engine for storage times less than 1 day, and salt has the great advantage of being liquid, thus enabling heat transfer by counterflow, minimizing entropy creation. Solar salt has a well-known list of other advantages such as low vapor pressure, high compatibility with steels, and environmental friendliness. It does not disintegrate in response to thermal cycling stresses the way a solid would. It creates no explosion hazard.

The $NaNO_3/KNO_3$ phase diagram is shown in Fig. 3.[26–28] At the eutectic composition (0.5 M fraction of $NaNO_3$), the melting temperature is 495 K (220 °C), about the same as an ordinary Pb/Sn solder. There is also a decomposition boundary at approximately 823 K (550 °C), a temperature conveniently near the steel creep cliff shown in Fig. 1.[29–32] The decomposition boundary is the point where the performance becomes difficult to predict, not where the salt begins to fail. The first stages of NO_3 decomposition are reversible and occur via the nitrate/nitrite reaction $2NO_3^- \rightarrow 2NO_2^- + O_2$. Approximately 3% of the nitrate has converted into nitrite at 823 K (550 °C).[29] The kinetics of outgassing and re-absorption of O_2 have been measured and found not to be unduly rapid.[30,31] Nitrogen oxide and N_2 evolve irreversibly at high rates above 923 K (700 °C).[32] The true upper operating temperature of solar salt exposed to air is not presently known.[32] The corrosion of stainless steels by these salts is mild and amounts to approximately 10 μm per year at 823 K (550 °C), chiefly due to oxidation.[33,34]

Figure 4 shows the important thermophysical properties of solar salt over the temperature range of interest.[35–37]

C. Hydrocarbon cryogen

Equation (1) dictates that $T_1 - T_0$ is as large as possible and ξ is as small as possible. For reasons explained in detail in Sec. III, the properties of solar salt determine $T_1^+ = 823\text{K}$ and

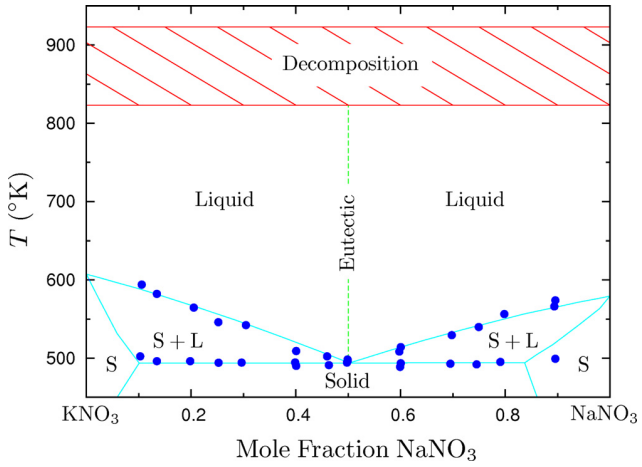

FIG. 3. The $NaNO_3/KNO_3$ phase diagram, after Rogers and Janz.[26] The measurements of the liquidus and solidus lines are from Rogers and Janz and also Kramer and Wilson.[27] The lines are theory due to Zhang *et al.*[28] The eutectic freezing temperature is 495 K (222 °C). The decomposition temperature is 823 K (550 °C).[29–32]

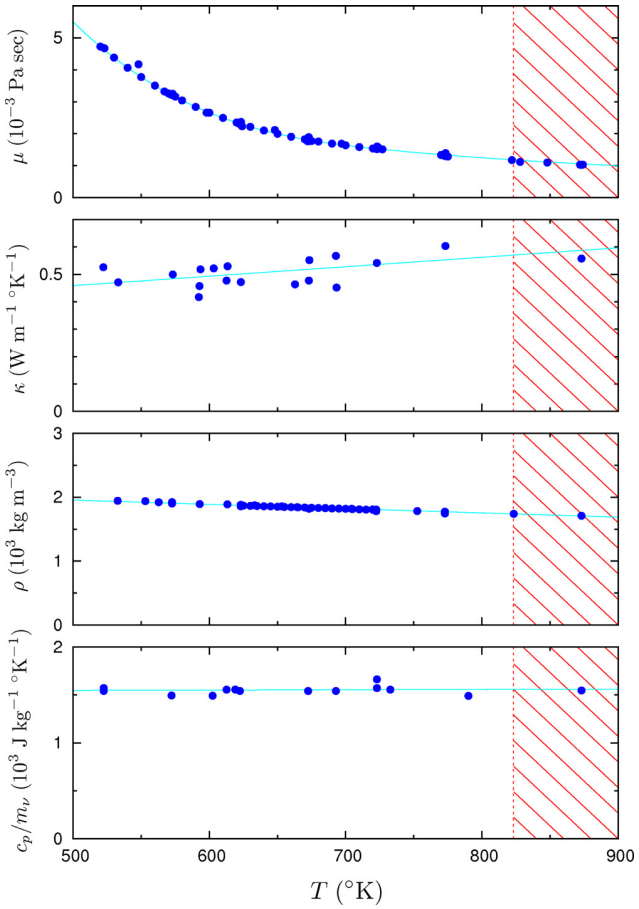

FIG. 4. Thermophysical properties of $NaNO_3/KNO_3$ eutectic. The viscosity data are from Janz *et al*. as supplemented by Lasfargues *et al*.[35,36] The solid line is the fit of Janz *et al*. splined at 730 K to a power series in $1/T$. The remaining data and the interpolations through them are from Bauer *et al*.[37] The molar mass per formula unit is $m_\nu = 0.094\,\text{kg mol}^{-1}$. The equipartition heat capacity is $c_p^{ideal}/m_\nu = 15R/m_\nu = 1330\,\text{J K}^{-1}\,\text{kg}^{-1}$. For comparison, room-temperature water has $\mu = 0.001\,\text{Pa s}$, $\kappa = 0.59\,\text{W m}^{-1}\,\text{K}^{-1}$, $\rho = 1000\,\text{kg m}^{-3}$, and $c_p/m_\nu = 4810\,\text{J kg}^{-1}\,\text{K}^{-1}$.

$T_1 = 495\,\text{K}$, and thus, $\xi = T_1^+/T_1 = 1.66$. It remains to maintain T_0 as low as possible. However, once T_0 gets so low that $T_0^+ < T_1$, these two temperatures effectively switch roles. T_0^+ must then be greater than T_{dump} since there would otherwise be no way to re-initialize the engine after it had stopped and equilibrated with the environment. Thus, we have $T_0 = 300\,\text{K}/\xi = 180\,\text{K}$.

For the purposes of this paper, a second storage fluid will be prototyped as *n*-hexane. All fluids that remain liquid between 180 K and 300 K with vapor pressure less than 1 atm are hydrocarbons or derivatives of them, so their physical properties are similar; they all have health and safety issues that must be weighed. Hexane, a component of gasoline, is pervasive, biodegradable, and cheap, and it is widely used in the food industry for extracting oils from seeds, but it is also highly flammable and neurotoxic.[38–42] Anhydrous methanol, to which hexane is physically similar and which is an acceptable substitute, is vastly more toxic. All the lower alcohols—methanol, ethanol, propanol, and propylene glycol—are hygroscopic and become viscous, like honey, at cryogenic temperatures when mixed with water.[43,44] Hydrocarbons can be rendered flame-resistant through halogenation, and a fluid such as CH_2Cl_2 would work perfectly well although it would increase the stress on stratospheric ozone.[45,46]

Figure 5 shows the important thermophysical properties of *n*-hexane over the temperature range of interest.[47–53]

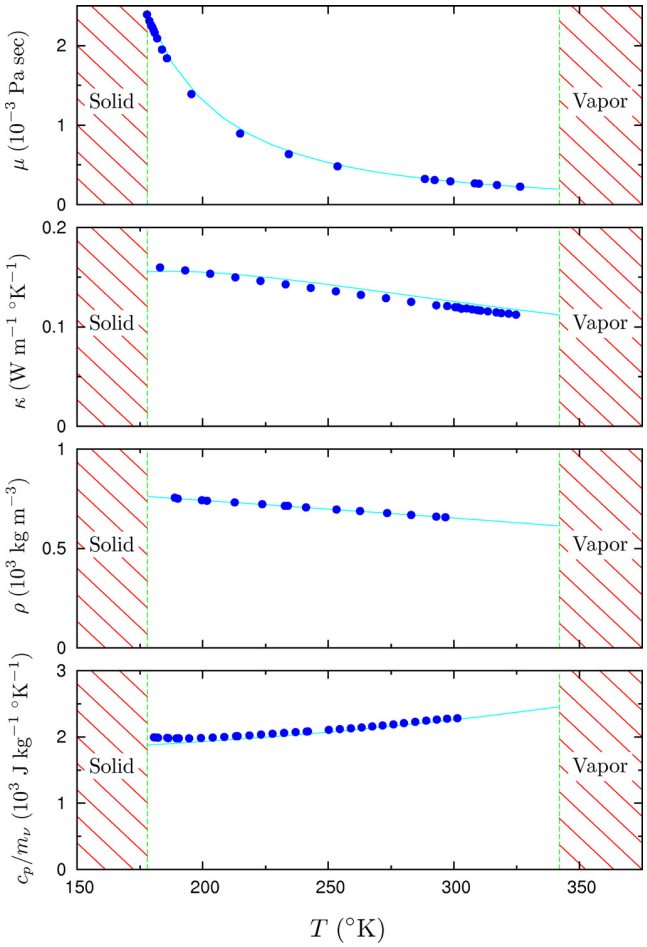

FIG. 5. Thermophysical properties of *n*-hexane (C_6H_{14}). The melting and boiling temperatures at 1 atm are 179 K and 350 K, respectively. The data are from various sources in the literature.[47–52] The lines are from the NIST standard reference database.[53] The temperature calibration of Giller and Drickamer has been adjusted 3% to agree with the accepted melting temperature.[49] The molar mass per formula unit is $m_\nu = 0.086\,\text{kg mol}^{-1}$. The equipartition capacity with hydrogen motion frozen is $c_p^{ideal}/m_\nu = 18R/m_\nu = 1740\,\text{J K}^{-1}\,\text{kg}^{-1}$.

D. Working fluid

The working fluid in this application is limited to gases that are extremely stable at high temperatures and far from liquefaction or solidification phase transitions at mildly cryogenic ones. The mechanical advantages of working near a critical point are outweighed in this case by danger of fluid raining or snowing out and damaging the turbine blades. This eliminates, in particular, CO_2, which has both liquefaction and freezing transitions in the range of 200–300 K. These considerations plus requirements of chemical inertness, cheapness, and environmental friendliness restrict the possibilities to Ar and N_2. The advantages of a lowered compression ratio and, potentially, higher adiabatic efficiency by using a gas with no internal degrees of freedom point to Ar as the preferred choice. However, N_2 has the advantage of requiring only minor modifications of rotor and stator airfoil shapes already optimized for use in air-breathing jet engines.[54]

Table II shows the thermophysical properties of Ar and N_2 over the temperature and pressure range of interest.[53] Both gases are functionally ideal (and thus polytropic) except at the lowest temperatures. The correct low-temperature equation of state must be used in fine-tuning the turbomachinery, but the ideal equation of state is sufficient for making efficiency and cost estimates.

TABLE II. Thermophysical properties of working fluids Ar and N_2.[53] Both gases approach their liquid-vapor critical points at the lowest temperatures but are otherwise highly ideal. The specific heat ratios $\gamma = c_p/c_v$ are well approximated by the equipartition values of 5/3 and 7/5. The molar masses m_ν of 0.040 kg mol^{-1} and 0.028 kg mol^{-1} affect both the viscosity μ and the thermal conductivity κ but cancel out in the Prandtl number $Pr = \mu c_p/(m_\nu \kappa)$, which lies close to the ideal value of $4\gamma/(9\gamma - 5)$ in both cases.

Ar	$p = 1.0 \times 10^6$ Pa					$p = 3.55 \times 10^6$ Pa				
T (K)	μ (Pa s)	κ (W m^{-1} K^{-1})	$\rho RT/(m_\nu p)$	γ	Pr	μ (Pa s)	κ (W m^{-1} K^{-1})	$\rho RT/(m_\nu p)$	γ	Pr
180	1.482×10^{-5}	1.178×10^{-2}	1.041	1.769	0.715	1.620×10^{-5}	1.406×10^{-2}	1.180	2.167	0.872
240	1.898×10^{-5}	1.501×10^{-2}	1.014	1.716	0.685	1.981×10^{-5}	1.634×10^{-2}	1.055	1.857	0.731
300	2.286×10^{-5}	1.801×10^{-2}	1.005	1.695	0.676	2.347×10^{-5}	1.903×10^{-2}	1.019	1.771	0.696
398	2.865×10^{-5}	2.251×10^{-2}	0.999	1.681	0.670	2.908×10^{-5}	2.329×10^{-2}	0.999	1.718	0.676
495	3.385×10^{-5}	2.656×10^{-2}	0.997	1.675	0.668	3.418×10^{-5}	2.720×10^{-2}	0.992	1.697	0.670
659	4.174×10^{-5}	3.269×10^{-2}	0.996	1.671	0.667	4.198×10^{-5}	3.321×10^{-2}	0.990	1.681	0.666
823	4.724×10^{-5}	3.700×10^{-2}	0.996	1.667	0.666	4.749×10^{-5}	3.753×10^{-2}	0.989	1.673	0.665

N_2	$p = 1.0 \times 10^6$ Pa					$p = 6.52 \times 10^6$ Pa				
T (K)	μ (Pa s)	κ (W m^{-1} K^{-1})	$\rho RT/(m_\nu p)$	γ	Pr	μ (Pa s)	κ (W m^{-1} K^{-1})	$\rho RT/(m_\nu p)$	γ	Pr
180	1.208×10^{-5}	1.752×10^{-2}	1.033	1.462	0.759	1.489×10^{-5}	2.465×10^{-2}	1.238	2.010	0.990
240	1.519×10^{-5}	2.205×10^{-2}	1.010	1.429	0.735	1.667×10^{-5}	2.597×10^{-2}	1.051	1.607	0.794
300	1.804×10^{-5}	2.617×10^{-2}	1.002	1.417	0.728	1.909×10^{-5}	2.900×10^{-2}	1.002	1.509	0.753
398	2.224×10^{-5}	3.232×10^{-2}	0.998	1.406	0.724	2.297×10^{-5}	3.427×10^{-2}	0.979	1.450	0.734
495	2.598×10^{-5}	3.804×10^{-2}	0.996	1.396	0.724	2.654×10^{-5}	3.952×10^{-2}	0.973	1.422	0.729
659	3.162×10^{-5}	4.742×10^{-2}	0.996	1.377	0.727	3.203×10^{-5}	4.847×10^{-2}	0.973	1.389	0.730
823	3.666×10^{-5}	5.658×10^{-2}	0.997	1.358	0.732	3.699×10^{-5}	5.738×10^{-2}	0.975	1.365	0.733

III. REGENERATION

The practical material limitations described in Sec. II require $T_0^+ < T_1$. As shown in Fig. 6, this condition causes heat transfers on the high-pressure and low-pressure sides of the circuit to overlap, thus eliminating the need to actually transfer heat to or from the storage fluids over this temperature range. Instead, heat may simply be transferred directly from one side of the circuit to the other through a gas-gas heat exchanger, referred to as a regenerator, or a recuperator.[58] In the limit that the entropy generation by the heat exchangers is zero, regeneration has no effect at all on the round-trip efficiency but simply reduces the amount of heat exchanger steel required. It also reduces the temperature ranges over which the storage fluids are required to be liquid. A modified version of Fig. 1 with regeneration included is shown in Fig. 7.

Figures 6 and 7 clarify why T_0^+ cannot exceed T_{dump}. An engine powered down and equilibrated to T_{dump} could easily be re-initialized by heating the (frozen) solar salt from T_{dump} to T_1, but it could not be easily re-initialized if T_0^+ had to be cooled to a value less than T_{dump}.

Figure 6 justifies choosing T_1 to be the solar salt melting point. With T_1^+ and T_0^+ fixed at the solar salt decomposition temperature and ambient, respectively, Eq. (1) is maximized when $\xi \ln(\xi)/\xi - 1)$ is minimized. However, it may be seen from the plot of this function in Fig. 8 that the minimum occurs when $\xi \to 1$. Other costs not included in the calculation run away in this limit, so the specific value $\xi = 1$ is not meaningful. However, the convergence of the function itself to 1 in this limit has an important implication that there is no significant round-trip efficiency penalty for $1 < \xi < 2$. Virtually, any value of ξ in this range will do. Moreover, lowering T_1 degrades the efficiency rather than improving it. There is thus no efficiency advantage in employing specialty salts with lower melting temperatures.

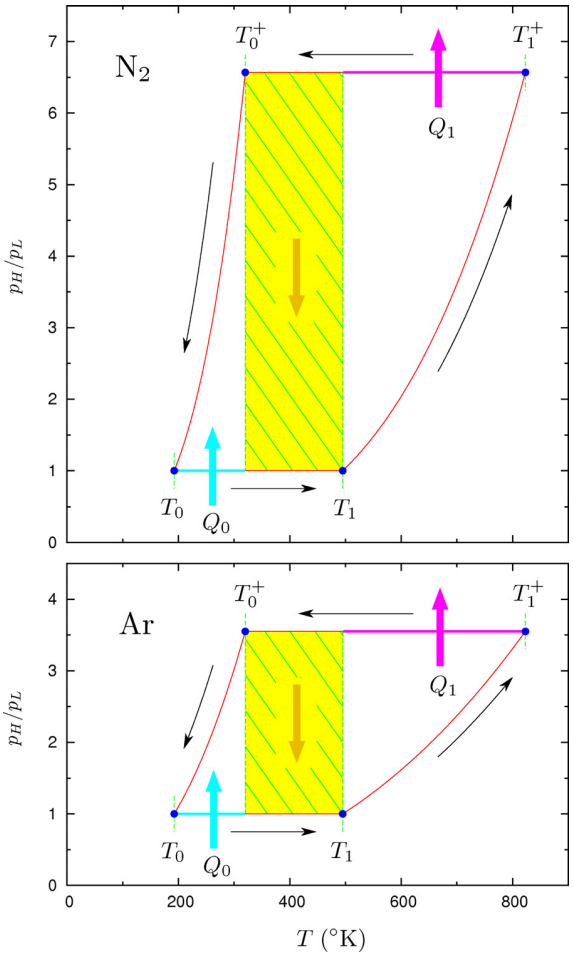

FIG. 6. Pressure-temperature diagrams for both Ar and N_2 working fluids. The parameters are those in Table I. The system is shown in the storage mode, following Fig. 1. Energy extraction is achieved by reversing all the heat and fluid flows. In the temperature range of $T_0^+ < T < T_1$ (hatched region), heat is transferred directly between the high-pressure and low-pressure sides of the circuit by means of a gas-gas heat exchanger. The remaining heat exchanges with storage fluids when ν moles of gas travel around the circuit are $Q_0 = \nu c_p T_0(\xi - 1)$ and $Q_1 = \nu c_p T_1(\xi - 1)$.

IV. ROUND-TRIP EFFICIENCY

A. Fictive temperature

The round-trip storage efficiency η_{store} is most simply computed through the entropy budget. The system entropy S must be the same before and after a storage cycle because it is a property of state, so any entropy ΔS generated during the cycle must be discarded as waste heat $T_{dump}\Delta S$, where T_{dump} is the slough temperature, roughly ambient. This heat represents a loss from the stored energy E_{store} that cannot be re-transmitted as grid power. We thus have

$$\eta_{store} < 1 - \frac{T_{dump}}{T_f} \quad \left(\frac{1}{T_f} = \frac{\Delta S}{E_{store}}\right). \tag{2}$$

The main contributions to the fictive temperature T_f come from the turbomachinery and three heat exchangers,

$$\frac{1}{T_f} = \frac{1}{T_f^{turbo}} + \sum \frac{1}{T_f^{hx}}. \tag{3}$$

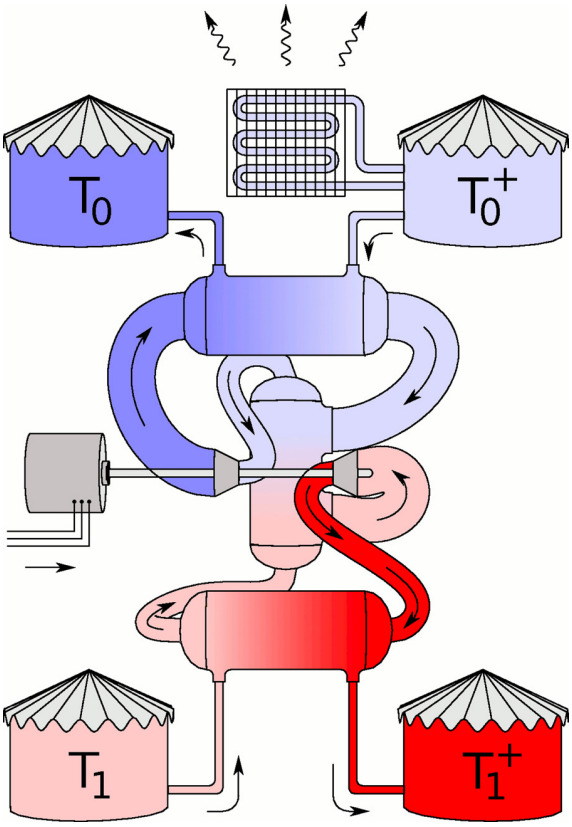

FIG. 7. Diagram of pumped thermal storage with heat exchange and regeneration. It is conceptually the same as Fig. 1 but has T_1 and T_0^+ reversed. The heat flows are as shown in Fig. 6.

Other losses such as generator/motor inefficiency, unmanaged turbulence, and viscous drag in the conduits are percent-level corrections.

B. Turbomachinery

In an adiabatic (entropy-conserving) compression or expansion, the temperature change dT resulting from a pressure change dp satisfies

$$\frac{dT}{T} = \left(\frac{\gamma - 1}{\gamma}\right) \frac{dp}{p}, \tag{4}$$

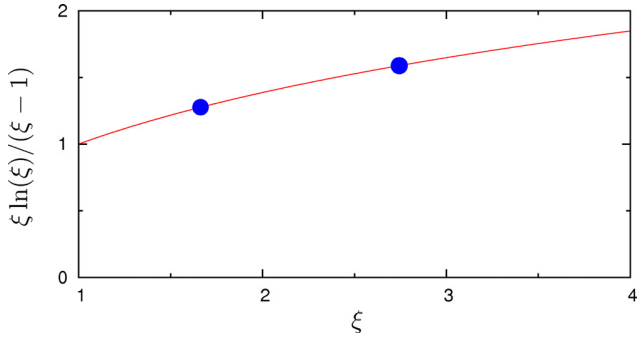

FIG. 8. Plot of the merit function $\xi \ln(\xi)/(\xi - 1)$ implicit in Eq. (1) with the values of T_0^+ and T_1^+ held fixed. The two circles correspond to $\xi = 823\,\text{K}/495\,\text{K} = 1.66$ and $\xi = 823\,\text{K}/300\,\text{K} = 2.74$. This shows that $NaNO_3/KNO_3$ eutectic is nearly optimal as a storage medium and that round-trip efficiency is actually degraded by the substitution of specialty salts with lower melting points.

where $\gamma = c_p/c_v$. In the limit that the turbomachinery is perfectly adiabatic, the temperature ratio ξ in Fig. 1 is thus related to the ratio of the upper and lower pressures p_h/p_l by

$$\xi = T_0^+/T_0 = T_1^+/T_1 = \left(\frac{p_h}{p_l}\right)^{(\gamma-1)/\gamma}. \tag{5}$$

In a real turbocompressor, Eq. (4) is modified to

$$\frac{dT}{T} = \frac{1}{\eta_c}\left(\frac{\gamma-1}{\gamma}\right)\frac{dp}{p}, \tag{6}$$

where η_c is the compressor polytropic efficiency. This slightly elevates the discharge temperature with respect to the ideal one for a given compression ratio. Integrating between the ideal temperature and the actual one at a constant pressure gives the entropy created when ν moles of gas pass through the compressor

$$\Delta S_c = \int \frac{\nu c_p}{T}\, dT = \nu c_p \left(\frac{1}{\eta_c} - 1\right)\ln(\xi). \tag{7}$$

From the version of Eq. (6) appropriate for the turbine

$$\frac{dT}{T} = \eta_t \left(\frac{\gamma-1}{\gamma}\right)\frac{dp}{p}, \tag{8}$$

one obtains similar entropy created when ν moles of gas expand through the turbine

$$\Delta S_t = \int \frac{\nu c_p}{T}\, dT = \nu c_p (1-\eta_t)\ln(\xi). \tag{9}$$

Since the energy stored by cycling ν moles of gas is $E_{store} = (T_1 - T_0)(\xi - 1)\nu c_p$, the inverse fictive temperature of the turbomachinery is

$$\frac{1}{T_f^{turbo}} = \frac{2(\Delta S_c + \Delta S_t)}{E_{store}} = \frac{2}{T_1 - T_0}\left(\frac{1}{\eta_c} - \eta_t\right)\frac{\ln(\xi)}{\xi - 1}. \tag{10}$$

The factor of 2 accounts for summing the entropy generated during the storage and extraction steps. Equation (1) is obtained by substituting this expression into Eq. (2).

The parameters of Table I give

$$T_f^{turbo} = 1210\,\mathrm{K}. \tag{11}$$

The values of η_c and η_t leading to this result lie at the extreme high end of present-day gas turbine technology.[59–63] They are benchmarked in the GE 90 aircraft engine. They are not characteristics of turbomachinery generally, however, so custom design is required to achieve them in practice. Turbomachinery bought off the shelf is a product fine-tuned to specific market needs that require a different set of compromises. There are theoretical indications that each η_c and η_t could be improved a further 1%.[64–67]

C. Heat exchangers

The fictive temperature of a heat exchanger differs from that of the turbomachinery depending on both the size and the power. The physical principles are elementary and equally applicable to all heat exchanger designs, so the simple shell-and-tube prototype of Fig. 9

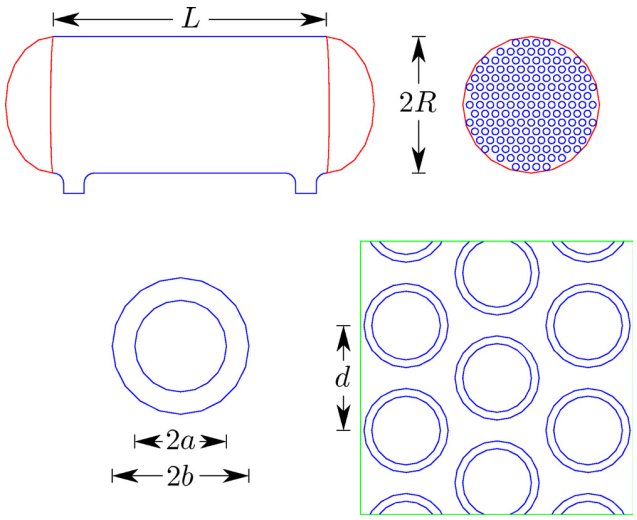

FIG. 9. Illustration of the shell-and-tube prototype for the heat exchanger. The number of tubes shown is $N = 151$. The lower right shows the case of $b/a = 1.224$ and $d/b = 1.25$. The lower left shows the case of $b/a = 1.491$.

suffices for estimating the amount of steel required to achieve a given fictive temperature, even if more advanced designs are actually employed.[70,71]

The laminar and turbulent cases are both important. The Reynolds number inside a heat exchanger tube is

$$Re = \frac{2}{N\pi a}\left(\frac{m_\nu \dot{\nu}}{\mu}\right), \tag{12}$$

where a is the tube's inner radius, N is the number of tubes, and $\dot{\nu}$ is the number of moles of working fluid passing through the circuit per unit time. The flow is laminar if $Re < 2000$, turbulent if $Re > 3000$, and intermittent otherwise. For this particular application, the effects of turbulence are adequately accounted for by replacing μ and κ in the laminar expressions by the Darcy-Weisbach formula[55,56]

$$\tilde{\mu} = \mu\left[\left(\frac{Re}{64}\right)f\right] \tag{13}$$

with the Swamee-Jain approximation for the Darcy friction factor

$$f = 0.25\left[\log_{10}\left(\frac{\epsilon}{7.4a} + \frac{5.74}{Re^{0.9}}\right)\right]^{-2} \tag{14}$$

and the Gnielinski correlation

$$\tilde{\kappa} = \kappa\left(\frac{11}{48}\right)\left[\frac{(f/8)(Re - 1000)Pr}{1.0 + 12.7(f/8)^{1/2}(Pr^{2/3} - 1)}\right], \tag{15}$$

where $Pr = \mu c_p/(m_\nu \kappa)$ is the Prandtl number. Figure 10 shows these modifications to μ and κ for various values of the tube surface roughness parameter ϵ.

The laminar case follows from elementary considerations. Assuming a pressure gradient $\partial p/\partial z$ along the tube and solving the Navier-Stokes equation

$$\mu\left(\frac{\partial^2}{\partial r^2} + \frac{1}{r}\frac{\partial}{\partial r}\right)v_z = \frac{\partial p}{\partial z} \tag{16}$$

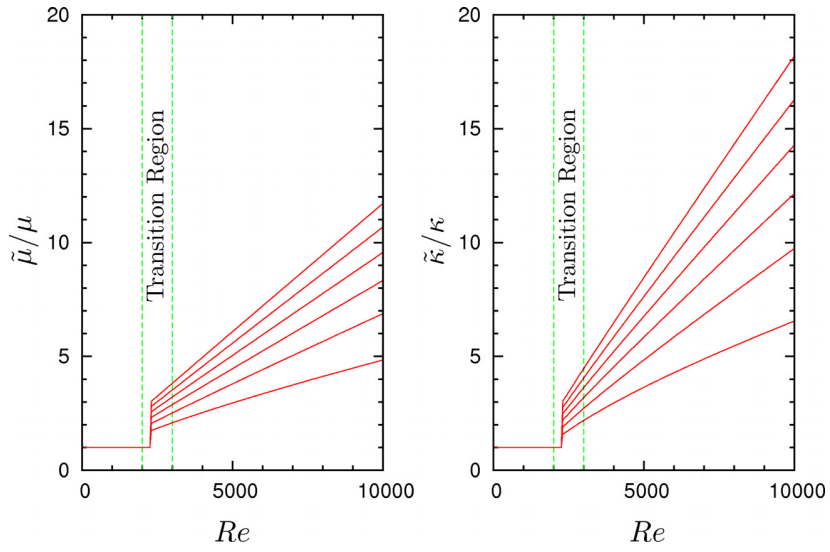

FIG. 10. Plot of turbulent enhancements of μ and κ defined by Eqs. (13) and (15) for $Pr = 2/3$ and surface roughness values $\epsilon/(2a) = 0.00$, 0.01, 0.02, 0.03, 0.04, and 0.05.

with a no-slip boundary condition, one obtains Hagen-Poiseuille flow

$$v_z = \frac{1}{4\mu}\left(\frac{\partial p}{\partial z}\right)(r^2 - a^2) \tag{17}$$

and an entropy generation due to viscous drag inside the tubes of

$$\dot{S}^{(in)}_{visc} = -\frac{2\pi N}{T}\int_0^a \left(\frac{\partial p}{\partial z}\right) v_z\, r dr = \left(\frac{8\mu}{\pi a^4}\right)\frac{TL}{N}\left(\frac{R\dot{\nu}}{p}\right)^2. \tag{18}$$

Assuming a temperature gradient $\partial T/\partial z$ along the tube and similarly solving the heat flow equation

$$\kappa\left(\frac{\partial^2}{\partial r^2} + \frac{1}{r}\frac{\partial}{\partial r}\right)\delta T = c_p\left(\frac{p}{RT}\right)\left(\frac{\partial T}{\partial z}\right)v_z, \tag{19}$$

one obtains the Graetz solution

$$\delta T = \frac{1}{\kappa}\left(\frac{\partial T}{\partial z}\right)\left(\frac{c_p\dot{\nu}}{N}\right)\frac{r^2(r^2 - 4a^2 + 3a^4)}{8\pi a^4} \tag{20}$$

from which the entropy generation due to the thermal resistance inside the tubes is computed to be

$$\begin{aligned}\dot{S}^{(in)}_{therm} &= -\frac{2\pi\kappa NL}{T^2}\int_0^a \left[\frac{\partial(\delta T)}{\partial r}\right]^2 rdr \\ &= \frac{11}{48\pi\kappa}\left(\frac{L}{N}\right)\left[\left(\frac{\partial T}{\partial z}\right)\frac{c_p\dot{\nu}}{T}\right]^2.\end{aligned} \tag{21}$$

These two contributions to $\dot{S}^{(in)}$ become equal when the heat exchanger length is L_0, defined by

$$\sqrt{\frac{384}{11}}\,\frac{\ell L_0}{a^2} = \left(\frac{\gamma}{\gamma - 1}\right)\frac{\Delta T}{T}, \tag{22}$$

where ΔT is the temperature difference between the two ends of the heat exchanger and

$$\ell = \frac{\sqrt{\kappa\mu T}}{p} \tag{23}$$

is the working fluid scattering mean free path.[57] The entropy creation outside the tube is a multiple of $\dot{S}^{(in)}$ obtained by solving Eqs. (16) and (19) numerically for a given value of d. The result is summarized in Table III. The fictive temperature is then

$$\frac{1}{T_f^{hx}} = \frac{11}{24\pi\kappa}\left[\frac{\Delta T}{T}\frac{1}{(T_1 - T_0)(\xi - 1)}\right]^2\left[1 + \frac{\dot{S}^{(out)}}{\dot{S}^{(in)}}\right]\left(1 + \frac{L^2}{L_0^2}\right)\frac{\dot{E}}{NL}, \tag{24}$$

where $\dot{E}$ is the engine power. The factor of 2 accounts for entropy creation during both the storage and extraction steps. Entropy creation due to heat flow in the steel is too small to matter in this application.

There is no need to make the heat exchanger fictive temperature more than about 30 times T_f^{turbo}. A set of parameters that give T_f^{hx} in this range for laminar flow is shown Table III. The important quantity for costing purposes is the steel mass per engine watt

$$\frac{M}{\dot{E}} = \rho_{steel}\,\pi(b^2 - a^2)L\left(\frac{N}{\dot{E}}\right). \tag{25}$$

Here, $N/\dot{E}$ is the number of tubes per engine watt, given by

$$\frac{N}{\dot{E}} = \frac{2}{\pi a\,Re}\left(\frac{m_\nu}{c_p\mu}\right)\frac{1}{(T_1 - T_0)(\xi - 1)} \tag{26}$$

per Eq. (12). Both $M/\dot{E}$ and T_f^{hx} remain unchanged if L is made smaller by keeping NL fixed (which requires lowering Re). Thus, Table III actually describes a family of designs with different aspect ratios but with similar performance characteristics.

Making L longer and keeping NL fixed push Re over the turbulence threshold. As shown in Table IV, this causes a 50% reduction in $M/\dot{E}$ for the same value of T_f. This occurs because the turbulent enhancement of the thermal conductivity matters more than the turbulent enhancement of the viscosity when $L < L_0$. Thus, the optimal design with respect to steel mass has Re just above the turbulence threshold. Further, cost compromise at this value of Re may result in shortening of L keeping N fixed, reducing both T_f and $M/\dot{E}$ proportionately.

The choice of tube inner and outer radii a and b has no effect on T_f if Re and L are held fixed (and if $L < L_0$), but it has a large effect on $M/\dot{E}$. Accordingly, the total cost of steel is minimized by making a as small as possible. The minimum value of b/a required for creep resistance is determined by

$$\frac{b^2 - a^2}{b^2 + a^2} \geq \frac{\Delta p}{\sigma_{max}}, \tag{27}$$

where Δp is the pressure difference between the inside and outside of the tube and σ_{max} is the maximum stress allowed in the tube steel, shown in Fig. 2. To this minimal, b/a must be added a mill tolerance margin, the default for which is a factor of 1.25 (12.5% of diameter), and a salt corrosion margin, which is 4.0×10^{-4} m for a 40-year lifespan.[68,69] Thus, it is impractical to make a much smaller than 1.5×10^{-3} m in the high-temperature heat exchanger. The regenerator and low-temperature heat exchanger may involve microchannel designs of $a = 5.0 \times 10^{-4}$ m, thus potentially lowering $M/\dot{E}$ in those cases.[70,71]

V. COST

The cost $\mathcal{C}$ of grid storage has two distinct metrics: the cost per engine watt $\partial\mathcal{C}/\partial\dot{E}$ and the cost per stored joule $\partial\mathcal{C}/\partial E$. The first is characteristic of the engine and depends only on how

TABLE III. Prototypical heat exchanger parameters for the laminar case. The inner radius a is set to the smallest size heat exchanger tubing available commercially from multiple sources. The base value of b/a is the sum of the pure stress component from Eq. (27), which is relatively small, and a milling tolerance factor of 11.2% taken from the Los Alamos Engineering Standards Manual PD342 for this size tube. This brings the tubes into compliance with ASME B31.3 which is stricter than normally required for heat exchanger applications.[68] (ASTM guidelines require manufacturers to control the tube wall width to at least 12.5% of the diameter.[69]) To this is added an extra 4.0×10^{-4} m for the salt heat exchanger as a corrosion margin. The value of d/b is fixed at the industry value of 2.5 except for the regenerator, where it is picked to minimize $\dot{S}^{(out)}/\dot{S}^{(in)}$. The Reynolds number Re is set to just below the turbulence threshold. The value of L is then adjusted to make $T_f^{hx} \simeq 30\,000$. The extra significant figures in this table are included to aid in checking calculations and are not predictive.

Ar	Low	Regen.	High
T	240 K	398 K	659 K
ΔT	120 K	195 K	327 K
$p^{(\mathrm{in})}$	1.00×10^6 Pa	3.55×10^6 Pa	3.55×10^6 Pa
$p^{(\mathrm{out})}$	1.00×10^5 Pa	1.00×10^6 Pa	1.00×10^5 Pa
$\sigma_{\max}$	1.30×10^8 Pa	1.30×10^8 Pa	1.00×10^8 Pa
b/a	1.224	1.224	1.491
d/b	2.500	4.259	2.500
$\dot{S}^{(out)}/\dot{S}^{(in)}$	0.0182	0.6429	0.0119
ℓ	8.27×10^{-9} m	4.62×10^{-9} m	8.54×10^{-9} m
a	0.0015 m	0.0015 m	0.0015 m
L_0	55.2 m	96.5 m	54.6 m
L	20.0 m	30.0 m	20.0 m
Re	2000	2000	2000
$N/\dot{E}$	0.0997 W^{-1}	0.0651 W^{-1}	0.0463 W^{-1}
$M/\dot{E}$	0.0551 kg W^{-1}	0.0540 kg W^{-1}	0.0629 kg W^{-1}
T_f^{hx}	30 520 K	30 880 K	31 990 K
N_2	Low	Regen.	High
T	240 K	398 K	659 K
ΔT	120 K	195 K	327 K
$p^{(\mathrm{in})}$	1.00×10^6 Pa	6.52×10^6 Pa	6.52×10^6 Pa
$p^{(\mathrm{out})}$	1.00×10^5 Pa	1.00×10^6 Pa	1.00×10^5 Pa
$\sigma_{\max}$	1.30×10^8 Pa	1.30×10^8 Pa	1.00×10^8 Pa
b/a	1.224	1.224	1.491
d/b	2.500	5.047	2.500
$\dot{S}^{(out)}/\dot{S}^{(in)}$	0.0268	0.7943	0.0209
ℓ	8.97×10^{-9} m	2.72×10^{-9} m	4.91×10^{-9} m
a	0.0015 m	0.0015 m	0.0015 m
L_0	70.7 m	221.4 m	137.5 m
L	20.0 m	30.0 m	20.0 m
Re	2000	2000	2000
$N/\dot{E}$	0.0632 W^{-1}	0.0407 W^{-1}	0.0290 W^{-1}
$M/\dot{E}$	0.0350 kg W^{-1}	0.0338 kg W^{-1}	0.0393 kg w^{-1}
T_f^{hx}	29 540 K	28 050 K	32 150 K

fast energy is transferred to and from the grid, not on how much energy is stored or for how long. The second characterizes the storage medium and is completely independent of how fast energy is transferred in or out. One imagines first building the engine at a certain power rating (and cost) and then adding as much storage capacity as circumstances warrant.

A crude estimate of the cost per engine watt is

$$\frac{\partial \mathcal{C}}{\partial \dot{E}} = \frac{T_{GT}^{ex} - T_{dump}}{(T_1 - T_0)(\xi - 1)} \frac{\eta_{GT}}{1 - \eta_{GT}} \left(\frac{c_p^{N_2}}{c_p}\right) \left(\frac{p_0}{p_l}\right) \frac{\partial \mathcal{C}_{GT}}{\partial \dot{E}} + 2\,\frac{\partial \mathcal{C}_{steel}}{\partial M} \sum \frac{M}{\dot{E}}. \tag{28}$$

TABLE IV. The same as in Table III, except with the Reynolds number Re raised above the turbulence threshold in the smooth-tube limit ($\epsilon \to 0$). The quantities $\tilde{\ell}$ and $\tilde{L}_0$ are the same as ℓ and L_0 except computed with the turbulence-enhanced values of $\tilde{\mu}$ and $\tilde{\kappa}$ defined by Eqs. (13) and (15). T_f^{hx} is also computed using $\tilde{\kappa}$.

Ar	Low	Regen.	High
T	240 K	398 K	659 K
ΔT	120 K	195 K	327 K
$p^{(\mathrm{in})}$	1.00×10^6 Pa	3.55×10^6 Pa	3.55×10^6 Pa
$p^{(\mathrm{out})}$	1.00×10^5 Pa	1.00×10^6 Pa	1.00×10^5 Pa
$\sigma_{\max}$	1.30×10^8 Pa	1.30×10^8 Pa	1.00×10^8 Pa
b/a	1.224	1.224	1.491
d/b	2.500	4.258	2.500
$\dot{S}^{(out)}/\dot{S}^{(in)}$	0.0404	0.6429	0.0253
$\tilde{\ell}$	1.78×10^{-8} m	9.91×10^{-9} m	1.82×10^{-8} m
a	0.0015 m	0.0015 m	0.0015 m
$\tilde{L}_0$	25.7 m	45.0 m	25.6 m
L	20.0 m	30.0 m	20.0 m
Re	3000	3000	3000
$N/\dot{E}$	0.0665 W^{-1}	0.0434 W^{-1}	0.0309 W^{-1}
$M/\dot{E}$	0.0367 kg W^{-1}	0.0360 kg W^{-1}	0.0419 kg W^{-1}
T_f^{hx}	31 040 K	34 440 K	32 420 K
N_2	Low	Regen.	High
T	240 K	398 K	659 K
ΔT	120 K	195 K	327 K
$p^{(\mathrm{in})}$	1.00×10^6 Pa	6.52×10^6 Pa	6.52×10^6 Pa
$p^{(\mathrm{out})}$	1.00×10^5 Pa	1.00×10^6 Pa	1.00×10^5 Pa
$\sigma_{\max}$	1.30×10^8 Pa	1.30×10^8 Pa	1.00×10^8 Pa
b/a	1.224	1.224	1.491
d/b	2.500	5.047	2.500
$\dot{S}^{(out)}/\dot{S}^{(in)}$	0.0610	0.7942	0.0399
$\tilde{\ell}$	1.95×10^{-8} m	5.91×10^{-9} m	1.07×10^{-8} m
a	0.0015 m	0.0015 m	0.0015 m
$\tilde{L}_0$	32.5 m	101.7 m	63.3 m
L	20.0 m	30.0 m	20.0 m
Re	3000	3000	3000
$N/\dot{E}$	0.0421 W^{-1}	0.0272 W^{-1}	0.0193 W^{-1}
$M/\dot{E}$	0.0233 kg W^{-1}	0.0225 kg W^{-1}	0.0262 kg W^{-1}
T_f^{hx}	33 920 K	39 800 K	44 280 K

The definitions of these parameters and their values are summarized in Tables I and V.[72–77] The idea behind this expression is that the turbomachinery should cost about the same as a present-day commercial gas turbine of the same size. Thus, one scales the present-day gas turbine cost by the number of moles per second $\dot{\nu}$ required to give the given power. The marginal cost of the (very large) heat exchangers required is estimated at 2 times the cost of the steel used to make them. This is unrealistically low in the context of present-day heat exchanger markets, but it is a reasonable expectation for large-volume production. This is consistent with $\$2\,\mathrm{kg}^{-1}$ implicit in the heat-exchanger price figures in the study by Loh *et al.*, assuming a tube width of 0.125 times the tube diameter, the standard ASME milling margin.[78]

A crude estimate for the marginal cost per stored joule is

$$\frac{\partial \mathcal{C}}{\partial E} = \frac{1}{(T_1 - T_0)(\xi - 1)} \left[\left(\frac{m_\nu^{salt}}{c_p^{salt}} \right) \frac{\partial \mathcal{C}_{salt}}{\partial M} + \left(\frac{m_\nu^{hex}}{c_p^{hex}} \right) \frac{\partial \mathcal{C}_{hex}}{\partial M} \right]. \tag{29}$$

TABLE V. Top: Parameters used in Eq. (28) to estimate the cost per engine watt $\partial\mathcal{C}/\partial\dot{E}$. The total fictive temperature T_f is computed with Eq. (3) using values in Table IV. The total mass per engine watt $\sum M/\dot{E}$ is obtained by summing the values in Table IV. The standard gas turbine exhaust temperature T_{GT}^{ex} and thermodynamic efficiency η_{GT} are from Brooks.[72] The gas turbine cost per engine watt $\partial\mathcal{C}_{GT}/\dot{E}$ is from Black and Veach, as reported by NREL.[73] The Black and Veach cost of $0.60\,\mathrm{W}^{-1}$ for a simple cycle power plant upon which this estimate is based also agrees with Tidball *et al.*[74] The cited steel tubing price per kilogram $\partial C/\partial M$ is on the extreme low edge of the market range. Fenton quotes $\$0.6\,\mathrm{kg}^{-1}$ as the carbon steel price.[75] The price of stainless steel is typically 5 times the price of carbon steel. Bottom: Parameters used in Eq. (29) to estimate the marginal cost per stored joule $\partial\mathcal{C}/\partial E$. The nitrate eutectic cost per kilogram $\partial\mathcal{C}_{salt}/\partial M$ is from Apodaca.[76] The hexane cost per kilogram $\partial\mathcal{C}_{hex}/\partial M$ is taken to be the price of gasoline reported by the U.S. EIA.[77]

	Ar	N_2
T_f	1089 K	1107 K
$\sum M/\dot{E}$	$0.1136\,\mathrm{kg\ W}^{-1}$	$0.0720\,\mathrm{kg\ W}^{-1}$
T_{GT}^{ex}	873 K	823 K
η_{GT}	0.38	0.038
$\partial\mathcal{C}_{GT}/\partial\dot{E}$	$\$0.25\ \mathrm{W}^{-1}$	$\$0.25\ \mathrm{W}^{-1}$
$\partial\mathcal{C}_{steel}/\partial M$	$\$1.00\,\mathrm{kg}^{-1}$	$\$1.00\,\mathrm{kg}^{-1}$
$\partial\mathcal{C}/\partial\dot{E}$	$\$0.27\ \mathrm{W}^{-1}$	$\$0.20\ \mathrm{W}^{-1}$
$\partial\mathcal{C}_{salt}/\partial M$	$\$0.61\,\mathrm{kg}^{-1}$	$\$0.61\,\mathrm{kg}^{-1}$
$\partial\mathcal{C}_{hex}/\partial M$	$\$0.70\,\mathrm{kg}^{-1}$	$\$0.70\,\mathrm{kg}^{-1}$
$\partial\mathcal{C}/\partial E$	$\$3.54\times10^{-6}\,\mathrm{J}^{-1}$	$\$3.54\times10^{-6}\,\mathrm{J}^{-1}$

The definitions of these parameters and their values are summarized in Tables I and V. The idea behind this expression is that the asymptotic cost per stored joule is simply the cost of the medium in which it is stored. Specifically omitted from this estimate because they are too small to matter are the costs of large storage tanks ($\$50\,\mathrm{m}^{-3}$) and excavation ($\$2.4\,\mathrm{m}^{-3}$).[78–80]

Equations (28) and (29) are oversimplified, and they leave out many obvious costs—flow handling, cooling structures, tanks, insulation, pumps, site preparation, and small loss accounting. However, they are sufficiently accurate to reveal the broad-brush picture: the cost of the turbomachinery is lowered by the elevated pressure in the closed Brayton loop so much that the cost per engine watt becomes dominated by the cost of the heat exchangers. The latter are conceptually trivial and scale up easily to arbitrarily large sizes. They become arbitrarily efficient when they do. Heat exchangers large enough to contribute negligibly to the total entropy budget can be built for a total cost per engine watt comparable to that of a present-day simple-cycle gas turbine. The marginal cost per stored joule, dominated by the cost of the storage fluids, is about $\$3.54\times10^{-6}\,\mathrm{J}^{-1}$ ($12.7 per kWh).

The plant cost curves associated with Table V are shown in Fig. 11. With the understanding that these are only illustrations, on account of the large error bars, one can see that the cost

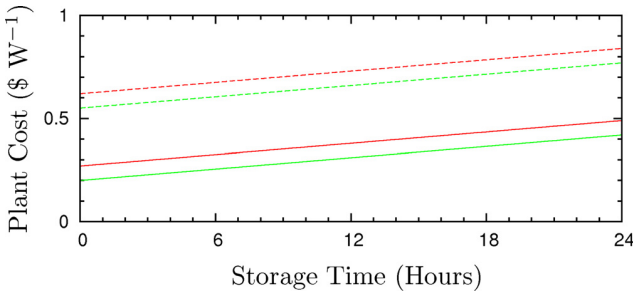

FIG. 11. Cost structure implicit in Table V. This should be understood as an illustration only because the error bars of Table V are very large. The base costs per engine watt $\partial\mathcal{C}/\partial\dot{E}$ for Ar and N_2 correspond to the two solid line intercepts at 0 h of storage time. The upper line is Ar. The slopes of these lines correspond to the marginal cost per stored joule $\partial\mathcal{C}/\partial E$. The dashed lines represent these quantities with $\$0.35\,\mathrm{W}^{-1}$ of infrastructure cost added (baffles, tanks, switchyard, buildings, etc.), the value needed to convert a $\$0.24\,\mathrm{W}^{-1}$ gas turbine into a full $\$0.6\,\mathrm{W}^{-1}$ simple-cycle power plant.[73,74]

of the storage is negligible for storage times less than a day and thus that only the costs per engine watt and plant infrastructure matter. There is, in particular, no significant economic advantage in substituting rocks for solar salt and hexane.

VI. DISCUSSION

A. Physical constraints

Which storage technology actually prevails in the end will depend ultimately on cost, and this is something difficult to assess correctly without actually building machines and testing them. Thus, it is not possible to make a purely economic case that the technology described here, which exists only as a concept, will win out. Rather the argument rests partly on such cost analysis as one can do combined with a little common sense.

It is highly reasonable, for example, from a physics perspective that the mechanical parts of thermal storage with heat exchange should cost less than pumped hydroelectric storage, the technology with which it is most closely related. The turbines are smaller by virtue of turning faster and having greater blade and fluid velocities. They require no burners or blade cooling. Salt and hexane store energy more compactly than water does when pumped uphill: one kg of water lifted 380 m, a typical pumped storage elevation drop, stores 0.7% of the energy that one kg of nitrate salt does when heated from T_1 to T_1^+. One kg of water falling 380 m transmits 3.4% of the energy to the turbine blades that 1 kg of Ar working fluid does when it travels around the Brayton circuit. In the case of N_2 working fluid, it is 1.7%. Thermal storage also uses less land than pumped hydroelectricity does—and, of course, requires no mountains or water supplies. This is shown explicitly in Fig. 12, where the footprint of a prototypical storage

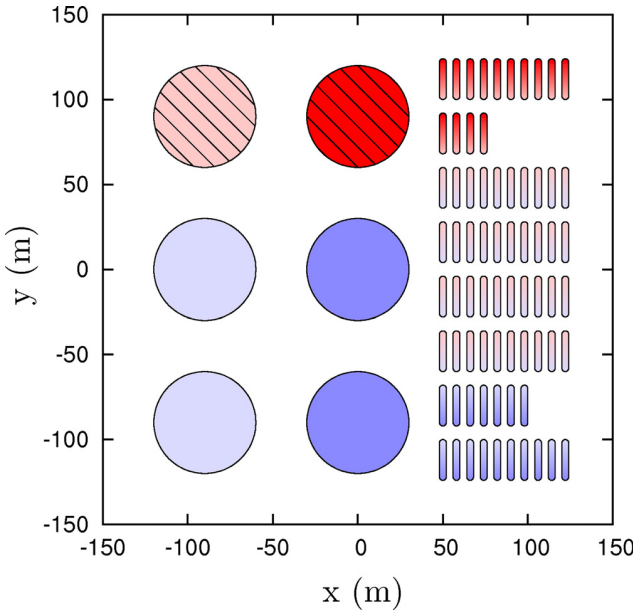

FIG. 12. Illustration of a thermal storage facility footprint showing the size scales involved. The parameters are those of Tables IV and V. The power is 2.5×10^8 W. The storage time is 24 h. The working fluid is Ar. The circles are oil depot storage tanks 14.0 meters tall and 30.0 m in radius.[79] The two hatched ones are for the nitrate salt (one each for two salt tanks in Figs. 1 and 7). The remaining four blue ones are for hexane. The heat exchanger units are cylinders of 20 m long and 2 m radius, ganged in parallel. The turbomachinery is too compact to be drawn meaningfully in this diagram, but the turbine, compressor, and generator together are about the size of one heat exchanger unit. The energy stored per unit of footprint is 2.5×10^8 J m^{-2} or about 2–10 times the typical pumped hydroelectric storage value, reckoned from the upper reservoir area.[81] For reasons of minimizing mechanical load cycling on the tanks, a realistic design would probably store the hot and cold salt in the same tank with a thermal barrier between them and similar to hexane, thus halving the number of tanks. The entire facility would also likely be underground, for thermal insulation reasons in the case of the tanks and for safety reasons in the case of the heat exchangers.

facility based on oil depot storage tanks is sketched out.[79] Depending on construction details, the thermal storage land requirement can be 10% or less than the equivalent pumped hydroelectric storage requirement, reckoned from the upper reservoir area.[81]

It is also reasonable that the heat exchangers should cost only slightly more than the steel used to make them. This is so even though large heat exchangers with the specifications in Table IV do not presently exist as products at any price. Heat exchangers are the mechanical engineering equivalent of semiconductor memory chips or flat-panel displays: one makes them by repeating the same simple step over and over again millions of times. This means that their manufacture can be automated. Their manufacture has not yet been automated, but this is only because there is no market for such products. It would be quite straightforward to program industrial robots to perform this task at an extremely low cost. A facility with the size shown in Fig. 12 would require about 3.0×10^7 tubes of length 20 m or a total length of 6.0×10^8 m, enough to circle the earth 15 times.

B. Heat versus electrochemistry

Were batteries ever to beat the marginal cost per stored joule of pumped hydroelectric storage, the comparison with the latter would become moot. However, they have not done so yet. The continued construction of new pumped storage facilities around the world demonstrates this.[82–85]

There are two reasons why the battery cost problem remains so intractable. One is that all batteries require an expensive internal infrastructure that cannot be eliminated without causing the battery to short and explode. The stored energy per unit mass of a battery varies between 1.4×10^5 J kg^{-1} for cheap lead-acid car batteries to 9.5×10^5 J kg^{-1} for high-end Li-ion batteries.[86–88] This is not significantly different from $c_p/m_\nu(T_1 - T_0)(\xi - 1) = 3.22 \times 10^5$ J kg^{-1} of nitrate salt, notwithstanding the fact that an active atom in a battery stores 10 times more energy than the atom of nitrate salt does. The extra mass is due to atoms that do not actually store any energy but guide electrons to the atoms that do. The second is that battery electrodes mechanically degrade, particularly if the battery is deeply cycled, thus creating long-term maintenance issues.[89] This occurs because the electrode surface, the place where electron motion converts into ion motion, is a scene of terrible violence on the scale of the atoms. Flow batteries and liquid metal batteries reduce the collateral damage of this violence, but they do so by means of engineering compromises that increase other costs.[90–93] It is not clear whether they will be cheaper than mass-produced Li-ion batteries.[94]

Batteries also have environmental issues associated with their metal ions that have led to mandatory recycling and the banning of household battery disposal in landfills.[95–99] This issue does not exist with pumped thermal storage with heat exchange. If the facility shown in Fig. 12 had a catastrophic tank breach (and no fire), the stored energy would dissipate harmlessly as heat, and the result would be a patch of cold nitrate fertilizer that could be easily cleaned up and re-used. If, on the other hand, a vanadium flow battery of the same capacity (two such tanks are required) had such a breach, 8.0×10^6 kg of vanadium ions would be dumped on the ground along with a comparable mass of sulfuric acid.

Thus, while batteries have an advantage over all other forms of storage at small scales in having no significant entry cost per engine watt, this advantage disappears once the scale becomes large enough that the cost entry barrier is surmounted.

C. Explosion danger

With the exception of hydrogen electrolysis, which has cost and electrode issues similar to batteries, all other methods for storing grid-scale energy have nuclear-scale explosion dangers.[100] This includes, in particular, flywheels, high pressure tanks, and all purely electrical media such as supercapacitors and superconducting magnetic coils.[101,102] These media also have lower energy storage densities, which is a secondary concern. In the case of flywheels and pressure vessels made out of steel, the maximum energy stored per unit mass of steel is $\sigma_{max}/\rho_{steel}$ or

about 2.5% of the energy stored thermally per unit mass of nitrate salt. For supercapacitors, this factor is about 10%.

Deliberately excluded from the list of explosive technologies is compressed air storage in underground caverns.[103,104] This is a special case both because it is underground (and thus not explosive) and because it is *physically equivalent* to thermal storage with heat exchange. It is well known that the energy expended in compressing any gas is stored in its heat. This is why adiabatically compressing N_2 from 1.0×10^5 Pa to 7.0×10^6 Pa (70 atmospheres), the typical underground storage pressure, raises its temperature from 300 K to 1101 K. Placing such hot gas underground just to cool off there would make no sense. Thus, all compressed air storage technologies with high round-trip efficiencies employ above-ground heat exchangers like those in Figs. 1 and 7 to cool the gas (extract energy from it) before pumping it underground.[105–109] Heat is then added back to the gas as it expands in the extraction step. The physical difference between underground storage and pure thermal storage with heat exchange is that the latter sends the working fluid through the Brayton cycle twice so as to eliminate the need to store working fluid at pressure at all—and thus to eliminate the need for the cavern.

Pumped thermal storage with heat exchange does have explosion danger. It is associated with the heat exchangers, however, not the storage media, so it scales with engine power rather than total stored energy. The parameters in Table IV give a total explosive energy of 90 s worth of generation at the design power, whatever it is, for Ar and 166 s for N_2. Thus, for the configuration of Fig. 12, the explosive power for Ar is 2.25×10^{10} J or 4.8 tons of TNT. Heat exchange units of this size and pressure are common in the petrochemical industry, and it is known that they explode rarely, but that when they do the result is catastrophic.[110] Thus, precautions must be taken to make sure that any tank explosion that might occur does not cascade, for example, by siting the units underground.

Another serious difficulty is the cost associated with managing the working fluid inventory in the case of breach. Both Ar and N_2 are asphyxiating gases. They are quite deadly until they dissipate in the atmosphere. The total working fluid inventory in the case of Fig. 12 is 2.7×10^5 kg of Ar. For comparison, the total amount of CO_2 released in the Lake Nyos disaster is estimated to be 10^9 kg.[111]

D. Additional technical issues

The power of pumped thermal storage with heat exchange is governed by adjusting the working fluid inventory up and down. The large heat capacity of the heat exchanger steel and corresponding slow thermal response call for regulating the storage fluid flow so as to keep the temperatures fixed. The power the working fluid delivers to the grid or absorbs from it is then directly proportional to the number of moles passing a given point per second. Since a motor/generator connected to the grid is phase-locked with other generators through electric forces propagating through the grid at the speed of light, the working fluid flow velocity is essentially fixed, and this means that one governs the power by reducing or increasing the background pressure of the working fluid in the circuit.

Two sets of turbomachinery may be required, one for storage and the other for extraction. For the parameters in Tables IV and V, this would increase the cost per engine watt by about $\$0.05\,W^{-1}$. In contrast to the situation in pumped hydroelectricity, the turbomachinery in this case cannot be automatically reversed because the blades are air foils carefully crafted for maximum efficiency under specific operating conditions, notably flow direction and Mach number. It is possible to design reversible airfoils, but it is not presently known how much efficiency compromise would be required to make machinery that worked equally well in both directions. The worst-case scenario is that no set of air foils would perform this task adequately, in which case two sets of turbomachinery would be required. The cost of doubling the turbomachinery becomes less and less of an issue as the pressure is raised.

The Brayton cycle requires closing. This is most conveniently accomplished using slightly different compression ratios for storage and generation, as shown in Fig. 13. Choosing these to

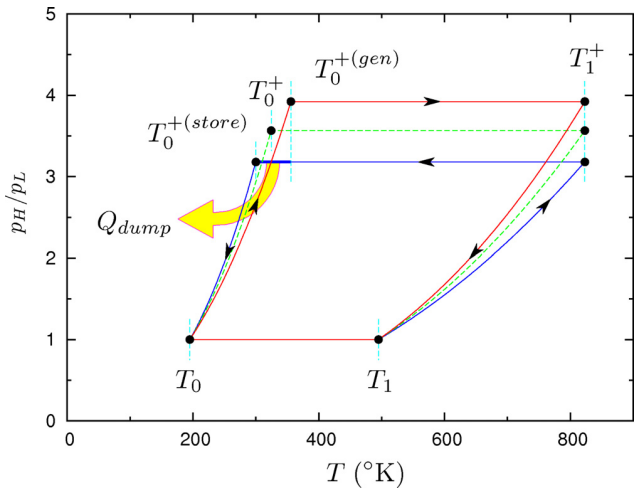

FIG. 13. Illustration of a fully closed Brayton cycle for the case of Ar working fluid. The storage and extraction cycles have their compression ratios modified to $\xi^{\eta_c\gamma/(\gamma-1)}$ and $\xi^{\gamma/(\gamma-1)\eta_t}$, respectively, so as to cause T_1^+ to match. This causes a mismatch between $T_0^{+(store)} = T_0\xi^{\eta_c\eta_t}$ and $T_0^{+(gen)} = T_0\xi^{1/\eta_c\eta_t}$. When ν moles of working fluid pass through a full storage/generation cycle, an amount of heat $Q_{store} = \nu c_p(T_0^{+(gen)} - T_0^{+(store)})$ must be sloughed off into the environment. This leads to Eq. (30).

make T_1^+ match causes the heat to be dumped at the lowest possible temperature. In place of Eq. (1), we then have

$$\eta_{store} < 1 - \frac{T_0}{T_1 - T_0}\left[\frac{\xi^{1/\eta_c\eta_t} - \xi^{\eta_c\eta_t}}{\xi - 1}\right]. \tag{30}$$

The parameters in Table I give $\eta_{store} < 0.75$, in agreement with Eq. (1). This number is too high, however, because $T_0^{+(store)}$ cannot lie below ambient. Taking ambient to be 300 K, we obtain $T_0 = 195$ K and thus $\eta_{store} < 0.72$.

In contrast to pumped hydroelectric and electrochemical storage, pumped thermal storage does not actually lose any energy but simply degrades it into heat that can be used for other things. For example, the rejection temperature $T_0^{+(gen)} = 356$K (82 °C) implicit in Fig. 13 is appropriate for preparing hot water. Cooling towers, such as those required for steam plants, are unnecessary in this case because there is no need to make a Rankine vacuum.[21] Simple thermal cooling ponds will do.

E. 19th century science

Insofar as the numbers I have presented in this paper are correct, they demonstrate that energy storage is a problem of 19th century science. No future laboratory breakthroughs or discoveries are required for solving it. All that is needed is fine engineering and assiduous attention to detail. Said poetically, this is 21st century rocket science.

Moreover, it is clear from Fig. 11 that the storage capacity of months becomes feasible once the engine (including the heat exchangers) exists as a product one can purchase at a known cost, particularly if the heat is further transferred into cheaper media for longer-term storage, such as rocks underground. Thus, pumped thermal storage with heat exchange is not a niche solution to the energy storage problem but a global one. This is the reason I think it will prevail.

ACKNOWLEDGMENTS

I wish to thank P. Larochelle, N. Cizek, J. Kesseli, T. Wolf, R. Apte, and T. Geballe for helpful discussions.

[1]D. Lindley, "The energy storage problem," Nature **463**, 18 (2010).
[2]R. M. Dell and D. A. J. Rand, "Energy storage—a key technology for global energy sustainability," J. Power Sources **100**, 2 (2001).
[3]Z. Luo, J. Wang, M. Dooner, and J. Clarke, "Overview of current development in electrical energy storage technologies and the application potential in power system operation," Appl. Energy **137**, 511 (2015).
[4]M. Carbajales-Dale, C. J. Barnhart, and S. M. Benson, "Can we afford storage? A dynamic net energy analysis of renewable electricity generation supported by energy storage," Energy Environ. Sci. **7**, 1538 (2014).
[5]D. Weissbach, G. Ruprecht, A. Huke, K. Czerski, S. Gottlieb, and A. Hussein, "Energy intensities, EROIs (Energy Return on Invested), and energy payback times of electricity generating power plants," Energy **52**, 210 (2013).
[6]E. Hittinger and R. Lueken, "Is inexpensive natural gas hindering the grid energy storage industry?," Energy Policy **87**, 140 (2015).
[7]G. Locatelli, E. Palerma, and M. Mancini, "Assessing the economics of large energy storage plants with an optimisation methodology," Energy **83**, 15 (2015).
[8]P. Denholm and M. Hand, "Grid flexibility and storage required to achieve very high penetration of variable renewable energy," Energy Policy **39**, 1817 (2011).
[9]*Renewable Energy Integration*, edited by L. E. Jones (Academic Press, New York, 2014).
[10]G. Swindle, *Valuation and Risk Management in Energy Markets* (Cambridge University Press, Cambridge, 2014).
[11]E. Barbour, G. Wilson, P. Hall, and J. Radcliffe, "Can negative electricity prices encourage inefficient electrical storage devices?," Int. J. Environ. Stud. **71**, 862 (2014).
[12]D. Droste-Franke, *Balancing Renewable Energy* (Springer Verlag, Heidelberg, 2012).
[13]J. Howes, "Concept and development of a pumped heat electricity storage device," Proc. IEEE **100**, 493 (2011).
[14]T. Desrues, J. Ruer, P. Marty, and J. F. Fourmogué, "A thermal energy storage process for large scale electric applications," Appl. Therm. Eng. **30**, 425 (2010).
[15]C. Périlhon, S. Lacour, P. Podevin, and G. Descombes, "Thermal electricity storage by a thermodynamic process: Study of temperature impact on the machines," Energy Procedia **36**, 923 (2013).
[16]A. Thess, "Thermodynamic efficiency of pumped heat electricity storage," Phys. Rev. Lett. **111**, 110602 (2013).
[17]A. White, G. Parks, and C. N. Markides, "Thermodynamic analysis of pumped thermal electricity storage," Appl. Therm. Eng. **53**, 291 (2013).
[18]National Academy of Sciences, National Academy of Engineering, and National Research Council, *Real Prospects for Energy Efficiency in the United States* (National Academies Press, Washington, DC, 2010), p. 280.
[19]R. L. Garwin and G. Charpak, *Megawatts and Megatons* (University of Chicago Press, Chicago, 2002).
[20]S. A. Wright, R. F. Radel, M. E. Vernon, G. E. Rochau, and P. S. Pickard, "Operation and analysis of a supercritical CO_2 Brayton cycle," Sandia National Laboratories, Report No. SAND2010-0171 (2010).
[21]A. S. Leyzerovich, *Steam Turbines for Modern Fossil Fuel Power Plants* (CRC Press, Boca Raton, FL, 2007).
[22]ASME, *2007 Boiler and Pressure Vessel Code (with Addenda for 2008)* (ASME, New York, 2007), Part II, Sec. D, Subpart 1, Tables 1A and 1B.
[23]H. Müller-Steinhagen, "Concentrating thermal power," Philos. Trans. R. Soc. A **371**, 20110433 (2013).
[24]R. W. Bradshaw and N. P. Siegel, "Molten nitrate salt development for thermal energy storage in parabolic trough solar power systems," Sandia National Laboratory, Report No. ES2008-54174 (2008).
[25]T. Bauer, D. Liang, and R. Tamme, "Recent progress in alkali nitrate/nitrite developments for solar thermal power applications," in *Molten Salts Chemistry and Technology*, edited by M. Gaune-Escard and G. M. Haarberg (Wiley, 2014).
[26]D. J. Rogers and G. J. Janz, "Melting-crystallization and premelting properties of $NaNO_3$–KNO_3 enthalpies and heat capacities," J. Chem. Eng. Data **27**, 424 (1982).
[27]C. M. Kramer and C. J. Wilson, "The phase diagram of $NaNO_3$–KNO_3," Thermochim. Acta **42**, 253 (1980).
[28]X. Zhang, J. Tian, K. Xu, and Y. Gao, "Thermodynamic evaluation of phase equilibria in Na NO_3–KNO_3 system," J. Phase Equilib. **24**, 441 (2003).
[29]D. A. Nissen and D. E. Meeker, "Nitrate/nitrite chemistry in $NaNO_3$–KNO_3 Melts," Inorg. Chem. **22**, 716 (1983).
[30]E. S. Freeman, "The kinetics of the thermal decomposition of potassium nitrate and of the reaction between potassium nitrite and oxygen," J. Phys. Chem. **60**, 1487 (1956).
[31]P. Gimenez and S. Fereres, "Effect of heating rates and composition on the thermal decomposition of nitrate based molten salts," Energy Procedia **69**, 654 (2015).
[32]R. I. Olivares, "The thermal stability of molten nitrite/nitrates salt for solar thermal energy storage in different atmospheres," Sol. Energy **86**, 2576 (2012).
[33]S. H. Goods and R. W. Bradshaw, "Corrosion of stainless steels and carbon steel by molten mixtures of commercial nitrate salts," J. Mater. Eng. Perform. **13**, 78 (2004).
[34]A. Kruizenga and D. Gill, "Corrosion of iron stainless steels in molten nitrate salt," Energy Procedia **49**, 878 (2014).
[35]G. L. Janz, U. Krebs, H. F. Siegenthaler, and R. P. T. Tomkins, "Molten salts: Volume 3, nitrates, nitrites, and mixtures," J. Phys. Chem. Ref. Data **1**, 581 (1972).
[36]M. Lasfargues, H. Cao, Q. Geng, and Y. Ding, "Rheological analysis of binary eutectic mixture of sodium and potassium nitrate and the effect of low concentration CuO nanoparticle addition to its viscosity," Materials **8**, 5194 (2015).
[37]T. Bauer, N. Pfleger, N. Breidenbach, M. Eck, D. Liang, and S. Kaesche, "Material aspects of solar salt for sensible heat storage," Appl. Energy **111**, 1114 (2013).
[38]Agency for Toxic Substances and Disease Registry, *Toxicological Profile for n-Hexane* (U.S. Department of Health and Human Services, 1999).
[39]P. Arlien-Søborg, *Solvent Neurotoxicity* (CRC Press, 1991).
[40]E. J. Conkerton, P. J. Wan, and O. A. Richard, "Hexane and heptane as extraction solvents for cottonseed: A laboratory-scale study," J. Am. Oil Chem. Soc. **72**, 963 (1995).
[41]H. Dominguez, M. J. Nuñez, and J. M. Lema, "Enzyme-assisted hexane extraction of soya bean oil," Food Chem. **54**, 223 (1995).

[42]A. Rosenthal, D. L. Pyle, and K. Niranjan, "Aqueous and enzymatic processes for edible oil extraction," Enzyme Microb. Technol. **19**, 402 (1996).
[43]T. W. Yergovich, G. W. Swift, and F. Kurata, "Density and viscosity of aqueous solutions of methanol and acetone from the freezing point to 10 °C," J. Chem. Eng. Data **16**, 222 (1971).
[44]F. A. M. M. Gonçalves, A. R. Trindade, C. S. M. F. Costa, J. C. S. Bernardo, and I. Johnson, "PVT, viscosity, and surface tension of ethanol: New measurements and literature data evaluation," J. Chem. Thermodyn. **42**, 1039 (2010).
[45]C. W. Kanolt, "Nonflammable liquids for cryostats," Sci. Pap. Bur. Stand. **20**, 619 (1925).
[46]R. Hossaini, M. P. Chipperfield, S. A. Montzka, A. Rap, S. Dhomse, and W. Fang, "Efficiency of short-lived halogens at influencing climate through depletion of stratospheric ozone," Nat. Geosci. **8**, 186 (2015).
[47]V. P. Brykov, G. K. Mukhamedzyanov, and A. G. Usmanov, "Experimental investigation of the thermal conductivity of organic fluids at low temperatures," J. Eng. Phys. **18**, 62 (1970) [Inzh.-Fiz. Zh. **18**, 82 (1970)].
[48]M. J. Assael, E. Charitidou, C. A. N. de Castro, and W. A. Wakeman, "The thermal conductivity of n-hexane, n-heptane, and n-decane by the transient hot-wire method," Int. J. Thermophys. **8**, 663 (1987).
[49]E. B. Giller and H. G. Drickamer, "Viscosity of normal paraffins near the freezing point," Ind. Eng. Chem. **41**, 2067 (1949).
[50]B. Knapstad, P. A. Skjølsvik, and H. A. Øye, "Viscosity of pure hydrocarbons," J. Chem. Eng. Data **34**, 37 (1989).
[51]B. Kalinowska, J. Jelińska, W. Wóycicki, and J. Stecki, "Heat capacities of liquids at temperatures between 90 and 300 K and at atmospheric pressure I. Method and apparatus, and the heat capacities of n-heptane, n-hexane, and n-propanol," J. Chem. Thermodyn. **12**, 891 (1980).
[52]H. Crauber, "Densitometer for absolute measurements of the temperature dependence of density, partial volumes, and the thermal expansitivity of solids and liquids," Rev. Sci. Instrum. **57**, 2817 (1986).
[53]E. W. Lemmon, M. O. McLinden, and D. G. Friend, "Thermophysical properties of fluid systems," in *NIST Chemistry Webbook, NIST Standard Reference Database Number 69*, edited by P. J. Linstrom and W. G. Mallard (U.S. National Institute of Standards and Technology, 2013).
[54]S. K. Roberts and S. A. Sjolander, "Effect of the specific heat ratio on the aerodynamic performance of turbomachinery," J. Eng. Gas Turbines Power **127**, 773 (2005).
[55]F. P. Incropera and D. P. DeWitt, *Fundamentals of Heat and Mass Transfer* (Wiley, 2006).
[56]B. J. Mckeon, C. J. Swanson, M. V. Zagarola, R. J. Donnelly, and A. J. Smits, "Friction factors for smooth pipe flow," J. Fluid Mech. **511**, 41 (2004).
[57]K. Huang, *Statistical Mechanics* (Wiley, 1963), p. 107.
[58]D. Beck and D. G. Wilson, *Gas Turbine Regenerators* (Springer, 2011).
[59]L. H. Smith, Jr., "Axial compressor aerodesign evolution at general electric," J. Turbomach. **124**, 321 (2002).
[60]A. R. Wadia, D. P. Wolf, and F. G. Haaser, "Aerodynamic design and testing of an axial flow compressor with pressure ratio of 23:3:1 for the LM2500+ gas turbine," J. Turbomach. **124**, 331 (2002).
[61]A. F. El-Sayed, *Aircraft Propulsion and Gas Turbine Engines* (CRC Press, 2008), p. 273.
[62]D. Eckhardt, *Gas Turbine Powerhouse*, 2nd ed. (Oldenbourg Wissenschaftsverlag, 2014), p. 152.
[63]J. K. Schweitzer and J. D. Smith, "Advanced industrial gas turbine technology readiness demonstration program: Phase II final report, compressor rig fabrication, assembly and test," U.S. Department of Energy, Report No. DOE/OR/05035-T2 (1981).
[64]D. K. Hall, E. M. Greitzer, and C. S. Tan, "Performance limits of axial turbomachine stages," in *Proceedings of the ASME Turbo Expo: Part A* (ASME, 2012), Vol. 8, p. 479.
[65]J.-M. Tournier and M. S. El-Genk, "Axial flow, multi-stage turbine and compressor models," Energy Convers. Manage. **51**, 16 (2010).
[66]M. P. Boyce, *Gas Turbine Engineering Handbook*, 4th ed. (Butterworth-Heinemann, 2011).
[67]L. M. Larosiliere, J. R. Wood, M. D. Hathaway, A. J. Medd, and T. Q. Dang, "Aerodynamic design study of advanced multistage axial compressor," National Aeronautics and Space Administration, Report No. NASA/TP-2002-211568 (2002).
[68]ASME, *ASME Code for Pressure Piping, B31: An American National Standard* (ASME, 2008).
[69]ASTM International, *Standard Specification for Seamless Carbon Steel Pipe for High Temperature Service* (American Society for Testing and Materials, ASME, 2006), Paragraph 16-3.
[70]A. Aquaro and M. Pieve, "High temperature heat exchangers for power plants: performance and advanced metallic recuperators," Appl. Therm. Eng. **27**, 389 (2007).
[71]N. Tsuzuki, Y. Kato, and T. Ishiduka, "High performance printed circuit heat exchanger," Appl. Therm. Eng. **27**, 1702 (2007).
[72]F. J. Brooks, "GE gas turbine performance characteristics," GE Power Systems, Report No. GER-3567H (2000).
[73]Black and Veach, *Cost and Performance Data for Power Generation Technologies* (U.S. National Renewable Energy Laboratory, 2012).
[74]R. Tidball, J. Bluestein, N. Rodriguez, and S. Knoke, "Cost and performance assumptions for modeling electricity generation technologies," U.S. National Renewable Energy Laboratory, Report No. NREL/SR-6A20-48595 (2010).
[75]M. D. Fenton, "Iron and steel," in *2013 Minerals Yearbook* (U.S. Geological Survey, 2015).
[76]L. E. Apodaca, "Nitrogen," in *2013 Minerals Yearbook* (U.S. Geological Survey, 2015).
[77]EIA, *Petroleum Marketing Monthly January 2016* (U.S. Energy Information Administration, 2016).
[78]H. P. Loh, J. Lyons, and C. W. White III, "Process equipment cost estimation: Final report," U.S. National Energy Technology Laboratory, Report No. DOE/NETL-2002/1169 (2002).
[79]API Standard 650, *Welded Steel Tanks for Oil Storage* (API Standard, 2012).
[80]B. Christensen, *Cost Estimating Guide for Road Construction* (U.S. Forest Service, Northern Region Engineering, U.S. Department of Agriculture, 2011).
[81]Task Committee on Pumped Storage of the Hydropower Committee of the energy Division of the American Society of Civil Engineers, *Compendium of Pumped Storage Plants in the United States* (ASCE, 1993).
[82]B. Dunn, H. Kamath, and J.-M. Tarascon, "Electrical energy storage for the grid: A battery of choices," Science **334**, 928 (2011).

[83]D. Rastler, "Electricity energy storage: Technology options," Electric Power Research Institute, Report No. 1020676 (2010).
[84]J. P. Deane, B. P. O. Gallachóir, and E. J. McKeogh, "Techno-economic review of existing and new pumped hydro energy storage plant," Renewable Sustainable Energy Rev. **14**, 1293 (2010).
[85]S. Rahman, L. M. Al-Hadhrami, and M. M. Alam, "Pumped hydro energy storage system: A technological review," Renewable Sustainable Energy Rev. **44**, 586 (2015).
[86]T. Reddy, *Linden's Handbook of Batteries*, 4th ed. (McGraw-Hill, 2010).
[87]K. E. Aifantis, S. A. Hackney, and R. V. Kumar, *High Energy Density Lithium Batteries: Materials, Engineering, Applications* (Wiley-VCH, 2010), p. 72.
[88]R. Van Noorden, "A better battery," Nature **507**, 26 (2014).
[89]E. M. Krieger, J. Cannarella, and C. B. Arnold, "A comparison of lead-acid and lithium-based battery behavior and capacity fade in off-grid renewable charging applications," Energy **60**, 492 (2013).
[90]G. I. Soloveichik, "Flow batteries: Current status and trends," Chem. Rev. **115**, 11533 (2015).
[91]A. Z. Weber, M. M. Mench, J. P. Meyers, P. N. Ross, J. R. Gostick, and Q. Liu, "Redox flow batteries: A Review," J. Appl. Electrochem. **41**, 1137 (2011).
[92]K. Gong, X. Ma, K. M. Conforti, K. J. Kuttler, J. B. Grunewald, K. L. Yeager, M. Z. Bazant, S. Gu, and Y. Yan, "A zinc-iron redox-flow battery under $100 per kWh of system capital cost," Energy Environ. Sci. **8**, 2941 (2015).
[93]H. Kim, D. A. Boysen, J. M. Newhouse, B. L. Spatocco, B. Chung, P. J. Burke, D. J. Bradwell, K. Jiang, A. A. Tomaszowska, K. Wang, W. Wei, L. A. Ortiz, S. A. Barriga, S. M. Poizeau, and D. R. Sadoway, "Liquid metal batteries: Past, present and future," Chem. Rev. **113**, 2075 (2013).
[94]D. I. Wood III, J. Li, and C. Daniel, "Prospects for reducing the processing cost of lithium ion batteries," J. Power Sources **275**, 234 (2015).
[95]G. Pistoia, J.-P. Wiaux, and S. P. Wolsky, *Used Battery Collection and Recycling* (Elsevier, 2001).
[96]*International Review of Experimental Pathology: Transition Metal Toxicity*, edited by G. W. Richter and K. Solez (Academic Press, 1990), Vol. 31.
[97]C. J. Rydh, "Environmental assessment of vanadium redox and lead-acid batteries for stationary energy storage," J. Power Sources **80**, 21 (1999).
[98]G. Majeau-Bettez, T. R. Hawkins, and A. H. Stromman, "Life cycle environmental assessment of lithium-ion and nickel metal hydride batteries for plug-in hybrid and battery electric vehicles," Environ. Sci. Technol. **45**, 4548 (2011).
[99]D. A. Notter, M. Grauch, R. Widmer, P. Wäger, A. Stamp, R. Zah, and A.-J. Althaus, "Contribution of Li-ion batteries to the environmental impact of electric vehicles," Environ. Sci. Technol. **44**, 6550 (2010).
[100]G. Saur and T. Ramsden, "Wind electrolysis: hydrogen cost optimization," U.S. National Renewable Energy Laboratory, Report No. NREL/TP-5600-50408 (2011).
[101]P. W. Parfomak, "Energy storage for power grids and electric transportation: A technology assessment," Congressional Research Service, CRS Report for Congress. Report No. R42455 (2012).
[102]A. A. Akhil, G. Huff, A. B. Currier, B. C. Kaun, D. M. Rastler, S. B. Chen, A. L. Cotter, D. T. Bradshaw, and W. T. Gauntlett, "DOE/EPRI electricity storage handbook in collaboration with NRECA," Sandia National Laboratory, Report No. SAND2013-5131 (2015).
[103]F. S. Barnes and J. G. Levine, *Large Energy Storage Systems Handbook* (CRC Press, 2011), p. 111.
[104]J. O. Goodson, "History of first U.S. compressed air energy storage (CAES) plant," Electric Power Research Institute, Report No. EPRI TR-101751 (1992).
[105]G. Grazzini and A. Milazzo, "A thermodynamic analysis of multistage adiabatic CAES," Proc. IEEE **100**, 461 (2012).
[106]E. Barbour, D. Mignard, Y. Ding, and Y. Li, "Adiabatic compressed air energy storage with packed bed thermal energy storage," Appl. Energy **155**, 804 (2015).
[107]W. Liu, L. Liu, L. Zhou, J. Huang, U. Zhang, G. Xu, and Y. Yang, "Analysis and optimization of a compressed air energy storage-combined cycle system," Entropy **16**, 3103 (2014).
[108]B. P. McGrail, C. L. Davidson, D. H. Bacon, M. A. Chamness, S. P. Reidel, F. A. Spane, J. E. Cabe, F. S. Knudsen, M. D. Bearden, J. A. Horner, H. T. Schaef, and P. D. Thorne, "Techno-economic performance evaluation of compressed air energy storage in the pacific northwest," Pacific Northwest National Laboratory, Report No. PNNL-22235 (2013).
[109]H. Safaei, D. W. Keith, and R. J. Hugo, "Compressed air energy storage (CAES) with compressors distributed at heat loads to enable waste heat utilization," Appl. Energy **103**, 165 (2013).
[110]CSB, *Case Study: Heat Exchanger Rupture and Ammonia Release in Houston, Texas* (U.S. Chemical Safety and Hazard Investigation Board, 2011).
[111]R. X. Faivre Pierret, P. Berne, C. Roussel, and F. Le Guern, "The lake Nyos disaster: Model calculations for the flow of carbon dioxide," J. Vulcanol. Geotherm. Res. **51**, 161 (1992).